BL11XU
QST Quantum Dynamics I

1. Introduction

BL11XU is an in-vacuum undulator beamline operated by the National Institutes for Quantum Science and Technology (QST). It is designed to provide scientists and engineers with a wide range of options for advanced synchrotron radiation and quantum functional material research. In BL11XU, switchable Si(111) and Si(311) double-crystal monochromators cooled by liquid nitrogen are installed in the optical hutch. Highly brilliant and well-collimated synchrotron X-rays are available in the energy range of 6–70 keV. There are four experimental hutches; each one contains specialized measurement instruments for studies involving Mössbauer spectroscopy (EH1), inelastic X-ray scattering and X-ray magnetic circularly polarized emission (EH2), surface X-ray diffraction (EH3), and Bragg coherent X-ray diffraction (EH4).

2. Mössbauer spectroscopy

The first experimental hutch is equipped with a nuclear resonance spectrometer that generates highly brilliant γ-rays from synchrotron radiation, the so-called synchrotron Mössbauer source (SMS). The SMS enables the local analysis of magnetic interactions, electronic states, and spin configurations of various functional materials. Recently, with the introduction of a new focusing mirror, the SMS has been used to measure small and thin-film samples using a beam that can focus the SMS down to 20 μm [1].

Recently, we have developed the first 3D Mössbauer surface analysis system by combining 2D mapping measurements using the focused SMS and depth-resolved conversion electron Mössbauer spectroscopy (DCEMS). As a demonstration experiment, we performed the 3D Mössbauer surface analysis of laser-ablated α-^{57}Fe foil [2]. DCEMS spectra were measured in three different energy regions: low energy (2–6.5 keV), medium energy (6.5–11 keV), and high energy (>11 keV). The depths correspond to 90, 60, and 30 nm, respectively. DCEMS scanning measurements were performed at different γ -ray irradiation positions on the surface of the iron foil.

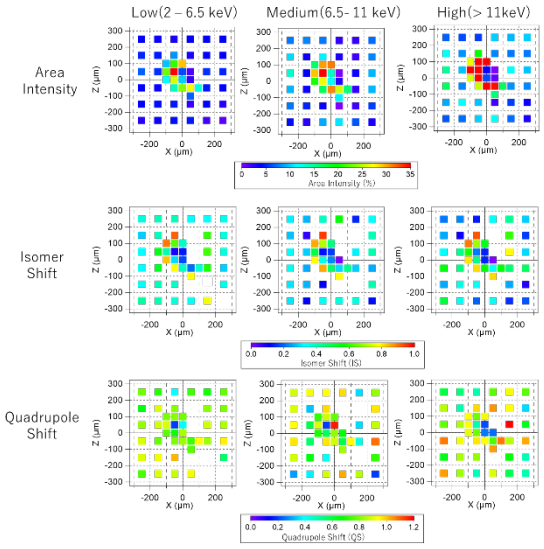

Fig. 1. Mapping of Mössbauer parameters (area intensity, isomer shift, and quadrupole shift) for the nonmagnetic phase modified by laser ablation.

Figure 1 shows the mapping of Mössbauer parameters (area intensity, isomer shift, and quadrupole shift) for the nonmagnetic phase modified by laser ablation. These results indicate that heterogeneous oxide ($Fe_{1-x}O$) formation occurs inside the iron foil. So far, we infer that the origin

of the heterogeneous spatial distribution of the nonmagnetic phase is the complicated detachment and scattering of molten fragments from the iron surface, caused by pulsed laser ablation. In this case, the scattered molten fragments may fall at irregular positions near the laser irradiation position and form iron oxides during resolidification. This surface oxidation would also be highly dependent on the laser heat density, cooling rate, and sample environment.

In the near future, this method will be a powerful analytical tool in the field of steel science, such as in the areas of corrosion, welding, and surface modification by laser ablation and peening.

3. Inelastic X-ray scattering

An inelastic X-ray scattering (IXS) spectrometer for hard X-rays installed in EH2 is used for resonant inelastic X-ray scattering (RIXS) at the K-edge of 3*d* transition metals and the L-edge of 5*d* transition metals. The optics of EH2 provides an energy resolution of 0.1–1 eV for both incident and scattered (emitted) X-rays. High-energy-resolution fluorescence-detected X-ray absorption spectroscopy (HERFD-XAS) and X-ray emission spectroscopy (XES) are also available using the spectrometer.

In FY2024, we installed a spherical diced Si(755) analyzer suitable for RIXS measurements at the Pt L_3-edge. In combination with an asymmetric Si(333) monochromator, a total energy resolution of 82 meV was achieved. Figure 2(a) shows the X-ray absorption spectrum of α-PtO_2. By tuning the incident X-ray energy near the absorption peak, resonantly enhanced electronic excitations with a maximum of around 3 eV were observed using the analyzer, as shown in Fig. 2(b). A band gap of approximately 1.6 eV [3] is clearly visible. Platinum is an important element in applications such as catalysis, and high-energy-resolution RIXS is expected to be a useful tool for operando measurements of subtle changes in electronic states.

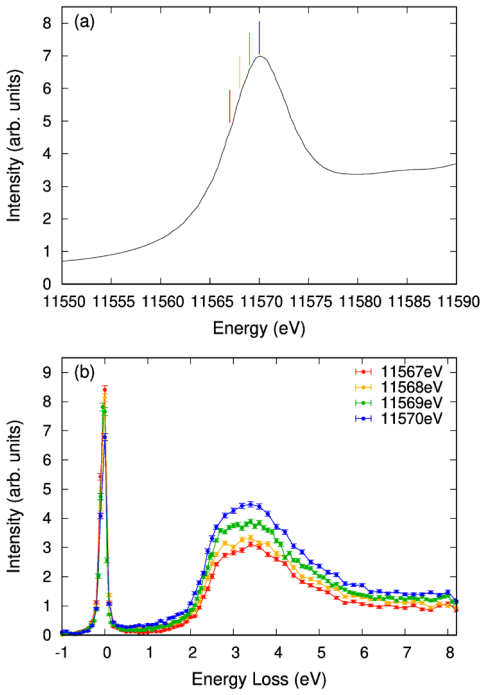

Fig. 2. (a) X-ray absorption spectrum of α-PtO_2. Vertical bars mark the incident X-ray energies used for RIXS measurements. (b) RIXS spectra of α-PtO_2 obtained with the spherical diced Si(755) analyzer.

4. X-ray magnetic circularly polarized emission

X-ray magnetic circularly polarized emission (XMCPE) is a phenomenon in which characteristic X-rays emitted from a magnetized material are circularly polarized [4]. An advantage of XMCPE is the large flipping ratio (~25%) in the hard X-ray region for 3*d* transition metal elements. This feature is well suited for observations of magnetic microstructures well below the sample surface.

The development of a bulk-sensitive magnetic microscope utilizing XMCPE started in FY2018 at BL11XU, and a scanning X-ray magnetic microscope with a lateral resolution of 10

μm was successfully constructed in FY2020 [5]. A depth-resolved measurement is also available [6]. With this microscope, magnetic domains in grain-oriented electrical steel have been investigated.

5. Surface X-ray diffraction

The third experimental hutch is equipped with a surface X-ray diffractometer integrated with a molecular beam epitaxy (MBE) chamber. This setup is designed for in situ investigations of III–V semiconductor surfaces, particularly focusing on surface crystallography under MBE conditions and the growth dynamics of multilayers and nanostructures. The III–V semiconductors studied include nitrides, such as GaN and InN, and arsenides, such as GaAs and InAs, which can be grown using two interchangeable types of MBE chambers.

Our recent research on nitride semiconductors is primarily aimed at elucidating the atomic-scale ordering that occurs at the interface between liquid gallium and the GaN(0001) surface under MBE conditions [7]. X-ray crystal truncation rod (CTR) scattering and reflection high-energy electron diffraction (RHEED) measurements were conducted before, during, and after Ga deposition onto the GaN surface (Fig. 3(a)). These measurements were repeated at various positions along the L index to obtain time-resolved CTR profiles along the 00 and 01 rods (Fig. 3(b)). The evolution of RHEED intensity was used to monitor Ga coverage on the GaN surface, enabling the extraction of CTR intensity profiles along the surface-normal direction.

Figures 3(c) and 3(d) show the impact of Ga deposition on the CTR profiles along the 00 and 01 rods, measured at a substrate temperature of 600 °C. The three-dimensional atomic coordinates and Ga coverage in each surface layer were obtained as fitting parameters in a least-squares analysis. As illustrated in Fig. 3(e), the initial GaN surface prior to Ga deposition consisted of either 0.3 monolayer (ML) of Ga (denoted as Layer 1) and 0.6 ML of Ga (denoted as Layer 0) on the N-terminated GaN(0001) surface. Upon Ga deposition, ordered Ga structures corresponding to a stable 2 ML interfacial configuration—comprising Layers 1 and 2—formed on the GaN(0001) surface, consistent with the previous theoretical model. Excess Ga beyond 2 ML was found to form droplets on Layer 2.

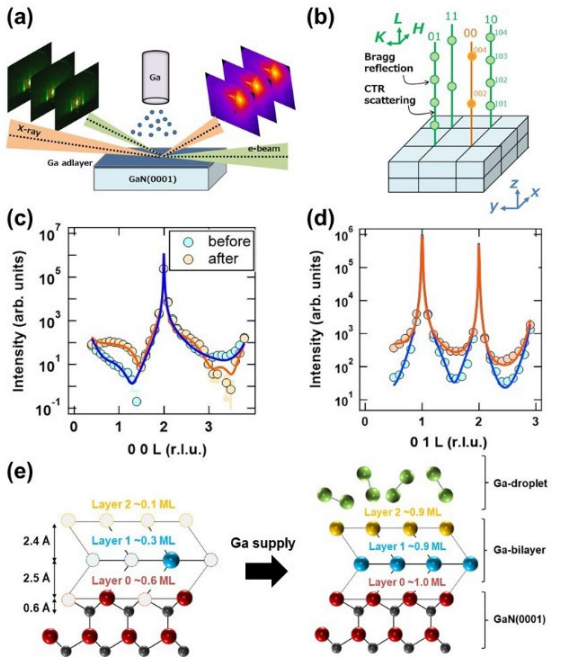

Fig. 3. Schematic of the (a) experimental setup and (b) characterized rods. Measured and simulated CTR profiles obtained before and after Ga supply along the (c) 00 and (d) 01 rods on GaN(0001). Each structure of Ga ordering (e) before and after Ga supply is based on the obtained lattice distances and Ga coverages.

6. Coherent X-ray diffraction

The fourth experimental hutch was newly

constructed to support coherent X-ray experiments and advanced quantum material evaluations. To ensure thermal stability, the hutch is equipped with high-performance insulation panels, and its floor has been reinforced and leveled to enhance mechanical precision. A newly installed diffractometer features a fully decoupled control system for sample and detector positioning, enabling stable diffraction measurements even for microscale samples. As part of this setup, a compact laser hutch has been attached externally to facilitate optically detected magnetic resonance (ODMR) measurements. This addition complements the main hutch by providing dual capabilities in diffraction and spectroscopy, offering a comprehensive platform for the structural and electronic characterization of quantum materials within a unified experimental environment.

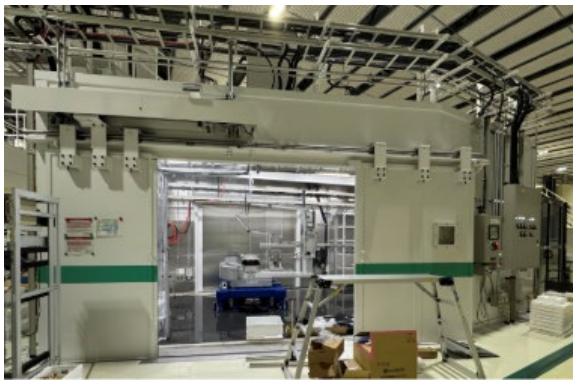

Fig. 4. Newly constructed fourth experimental hutch.

MITSUI Takaya[*1], FUJIWARA Kosuke[*1], ISHII Kenji[*2], INAMI Toshiya[*1], SASAKI Takuo[*3], OHWADA Kenji[*3], OSHIME Norihiro[*3], SHAO Mingyang[*3], MACHIDA Akihiko[*4], UENO Tetsuro[*2], and SUGAWARA Kento[*5]

[*1]Magnetism Research Group, Synchrotron Radiation Research Center, National Institutes for Quantum Science and Technology (QST)

[*2]Advanced Spectroscopy Research Group, Synchrotron Radiation Research Center, National Institutes for Quantum Science and Technology (QST)

[*3]Coherent X-ray Research Group, Synchrotron Radiation Research Center, National Institutes for Quantum Science and Technology (QST)

[*4]Hydrogen Materials Research Group, Synchrotron Radiation Research Center, National Institutes for Quantum Science and Technology (QST)

[*5]Beamline Operation Office, Synchrotron Radiation Research Center, National Institutes for Quantum Science and Technology (QST)

References:

[1] Fujiwara, K. Nakamura, S. Shimomura, S. & Mitsui, T. (2024). *JPS Conf. Proc.* **41**, 011002.

[2] Fujiwara, K. et al. (2024). *Appl. Phys. Express* **17**, 082002.

[3] Data retrieved from the Materials Project for PtO_2 (mp-617) from database version v2025.06.09 (DOI: 10.17188/1277905).

[4] Inami, T. (2017). *Phys. Rev. Lett.* **119**, 137203.

[5] Sugawara, K. Inami, T. Nakada, T. Sakaguchi, Y. & Takahashi, S. (2021). *J. Appl. Phys.* **130**, 113901.

[6] Inami, T. Sugawara, K. T. Nakada, T. Sakaguchi, Y. & Takahashi, S. (2021). *J. Appl. Phys.* **137**, 093901.

[7] Sasaki, T. et al. (2024). *Appl. Phys. Express* **17**, 025502.